V International Conference on Particle-based Methods – Fundamentals and Applications
PARTICLES 2017
P. Wriggers, M. Bischoff, E. Oñate, D.R.J. Owen, & T. Zohdi (Eds)

PATTERN FORMATION IN LAMINAR FLOW OF SUSPENSIONS THROUGH SQUARE CHANNELS

PHILIPPE SEIL[1], STEFAN PIRKER[2] AND THOMAS LICHTENEGGER[3]

[1] CD Laboratory for Multi-Scale Modelling of Multiphase Processes, Johannes Kepler University Linz
Altenbergerstrasse 69, 4040 Linz, Austria
philippe.seil@jku.at

[2] Department for Particulate Flow Modelling, Johannes Kepler University Linz

[3] Linz Institute of Technology (LIT), Johannes Kepler University Linz

Key words: Lateral Migration, Channel Flow, Suspensions, Lattice Boltzmann Method, Discrete Element Method

Abstract. The study of particulate suspensions flowing through narrow channels has received much attention in the last decades, especially with advance in the field of microfluidics devices. In square channels, it is known that particles in dilute suspensions migrate to equilibrium positions at the channel faces, and also at the channel corners for a channel Reynolds number above 260. However, most studies focused on very dilute systems, excluding particle-particle interactions. In this paper, we present simulations of suspensions with solid fractions up to 3%. In these simulations, we find two new patterns: at $\mathrm{Re}_{\mathrm{ch}} < 260$, the equilibrium positions split up and particles assume a staggered position, and at $\mathrm{Re}_{\mathrm{ch}} > 260$, the fraction of particles moving to the corner equilibrium positions increases with solid fraction. We present a characterization of these two effects and speculate about possible mechanisms leading to the formation of both patterns.

1 INTRODUCTION

The dynamics of particulate suspension flow through narrow channels features a broad variety of non-trivial phenomena. Over half a century ago, Segré and Silberberg [1] discovered that a neutrally buoyant, spherical particle in pipe flow migrates to an off-center equilibrium position located at $\approx 0.62 R_{\mathrm{pipe}}$ away from the pipe axis.

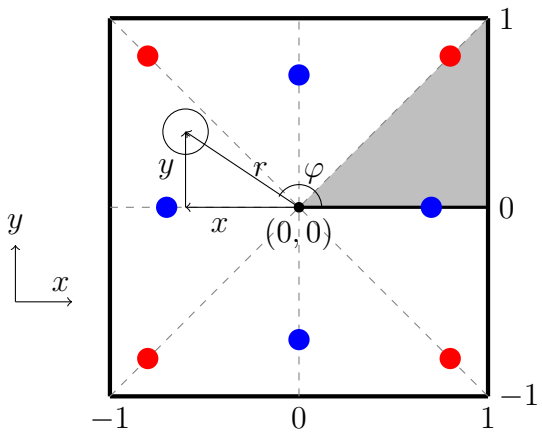

Figure 1: A sketch of the coordinate conventions used in the simulations. All results are given in coordinates normalized by $D/2$. In figs. 3 and 4, all final positions are mapped to the grey triangle. The dots indicate approximate locations of face (blue) and corner (red) equilibrium positions.

A similar effect exists for rectangular and square channels, where due to reduced symmetry only eight equilibrium positions are possible: four close to the channel corners, and four close to the channel faces (see fig. 1). Using simulations, Chun and Ladd [2] predicted that in a square channel at $\mathrm{Re}_{\mathrm{ch}} < 500$ particles move to all eight positions, while at $\mathrm{Re}_{\mathrm{ch}} \geq 500$ only the corner positions remain stable. However, through experiments, Di Carlo et al. [3, 4] found that at $\mathrm{Re}_{\mathrm{ch}} < 100$ only the face positions are stable. Miura et al. [5] examined cases with $\mathrm{Re}_{\mathrm{ch}} = 100 - 1000$, and found that the corner equilibrium positions only become stable above $\mathrm{Re}_{\mathrm{ch}} = 260$. All these experiments were done using very dilute systems, thus not much is known about denser systems. Matas et al. [6] investigated denser suspensions in pipe flow, and found trains of particles with an average spacing of $1.5 - 4.5 d_{\mathrm{p}}$ depending on the particle Reynolds number Re_{p}. Humphry et al. [7] and Kahkeshani et al. [8] also studied particle trains and preferred interparticle spacings, although in rather confined geometries. In this paper, we present simulations of flow of particulate suspensions through square channels. We investigate the influence of $\mathrm{Re}_{\mathrm{ch}}$ and solid fraction f_{s} on pattern formation, and present assumptions about possible underlying mechanisms.

2 METHODS AND SETUP

2.1 Computational Methods

We used a fully resolved[1] coupled approach between the lattice Boltzmann method (LBM) [9] and the discrete element method (DEM) [10] for our simulations. Using the method of Noble and Torczinsky [11], we have implemented, validated, and released this approach in the software *LBDEMcoupling* [12, 13]. Therefore, we give only a brief discussion of the numerical methods. For more thorough explanations, the reader is directed to the book by Krüger et al. [14] for the LBM and coupling methodology, and to the book by Pöschel and Schwager [15] for the DEM.

In the LBM, the fluid flow is simulated by solving the *LBGK* equation

$$f_i(\vec{x}+\vec{c}_i\Delta t, t+\Delta t) - f_i(\vec{x},t) = -(1-B)\underbrace{\frac{1}{\tau}\left(f_i(\vec{x},t) - f_i^{(eq)}(\vec{u},\rho)\right)}_{\text{BGK coll.}} + B\underbrace{\Omega_i^s(\vec{u}_s)}_{\text{solid coll.}} \quad (1)$$

on a regular grid for a set of particle distributions $\{f_i\}$. The $\{\vec{c}_i\}$ are a set of vectors to adjacent grid cells. In the present simulations, the *D3Q19* discretization scheme was chosen, which consists of six vectors to the nearest neighbours, twelve vectors to the second-next neighbours, and a zero vector. A timestep consists of two parts: collision and streaming. In the collision step, the left hand side of eq. (1) is applied to the $\{f_i\}$. This represents a tendency towards a local equilibrium distribution $f_i^{(eq)}(\vec{u},\rho)$ occurring at a timescale given by the relaxation time τ. In the streaming part, each population $f_i(\vec{x})$ is copied to the location $\vec{x}+\vec{c}_i$, which now has a set of off-equilibrium populations, and the simulation continues with the next collision step. Local density and velocity are given by

$$\rho = \sum_i f_i \qquad ; \qquad \rho\vec{u} = \sum_i \vec{c}_i f_i \quad (2)$$

and the pressure equation is solved by allowing for a slight compressibility: pressure differences are proportional to density differences. In eq. (1), the interaction with a solid covering a fraction B of the cell and moving at velocity $\vec{u}_s$ has also been included by blending between the BGK collision and an additional collision operator Ω_i^s [11].

[1] grid spacing $\Delta x <$ particle diameter d_p

The DEM [10] originates in molecular dynamics and is able to model the dynamics of systems consisting of single particles by integrating Newton's second law

$$m_i \ddot{\vec{x}}_i = \sum_{j \neq i} \vec{F}_{ij} + \vec{F}_i^{ext} \tag{3}$$

where $\vec{F}_{ij}$ is the interaction force between particles i and j, and $\vec{F}_i^{ext}$ are external forces due to gravity, hydrodynamic interactions, or other external influences. In the case of granular material, spring-dashpot interaction potentials of Hertz type are commonly used to model the particle-particle interaction. In this study, we used the model of Tsuji [16] and Antypov and Elliot [17]. Additional models for sliding [10] and rolling friction [18] were used to accurately depict the dynamics of interparticle collisions.

2.2 Simulation Setup

To ensure comparability to experiments, we chose a simulation setup that closely mimics the experiments of Miura et al. [5]. They used a square channel with edge length $D = 6\text{mm}$ and $L = 4\text{m}$. Consequently, we adopted the edge length and used periodic boundary conditions to create an infinite channel. A pressure gradient was applied using the periodic pressure boundary condition of Zhang and Kwok [19]. The particle diameter was $d_\text{p} = 650\mu\text{m}$, resulting in $\frac{D}{d_\text{p}} = 9.23$. Additional fluid parameters were kinematic viscosity $\nu = 1.6 \cdot 10^{-6}\text{m}^2/\text{s}$ and density $\rho = 1053\text{kg}/\text{m}^3$.

We used a resolution of $100 \times 100 \times 800$ grid cells for the simulation, resulting in a particle diameter of $10.8\Delta x$. A similar resolution was found to produce acceptable results in our validation tests [13]. We made sure that the Mach number did not exceed $\text{Ma} = 0.05$ to avoid compressibility errors in the LBM. The channel Reynolds number was defined as

$$\text{Re}_\text{ch} = \frac{D\bar{U}}{\nu} \tag{4}$$

with $\bar{U}$ being the average streamwise flow velocity. $\bar{U}$ was controlled by setting the pressure difference Δp between inlet and outlet. The channel was initialized to a product of two Poiseuille parabolas (in x and y direction) and a streamwise (z) linear pressure decrease. We investigated solid fractions of $f_\text{s} = 0.017\% \ldots 3\%$ ($N_\text{p} = 2 - 363$ particles) at $\text{Re}_\text{ch} = 60$, 190 and $f_\text{s} = 0.017\% \ldots 1\%$ ($N_\text{p} = 2 - 121$) at $\text{Re}_\text{ch} = 310$, 500. For each combination of Re_ch and f_s, between two and eight simulations with randomly generated initial configurations were carried out to achieve

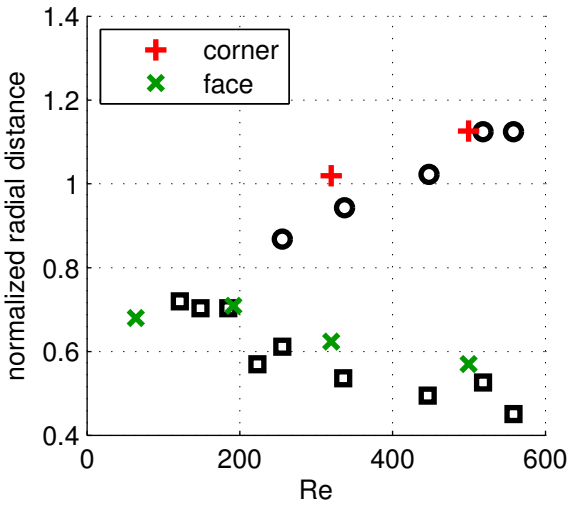

Figure 2: Radial distance of equilibrium positions from the channel centerline. Black circles and squares are corner and face positions found by Miura et al. [5]. Green "x" (face) and red "+" (corner) are our simulation results. Distance is normalized to $D/2$.

proper statistics.

3 RESULTS AND DISCUSSION

Just as in the experiments, the particles migrated to the two sets of equilibrium positions, except for the most dense cases ($f_s \geq 1\%$) where pattern formation broke down due to the high amount of interaction. Generally, migration happened in two stages: First, the particles moved out radially. Then, they tangentially migrated to their final positions. Typically, the second part of migration took longer than the first part. Our results are presented in more detail below. First, to give some validation, the most dilute cases are compared to experimental results. Then, we present two patterns found in denser cases.

3.1 Comparison to previous results

We now compare equilibrium positions found in the most dilute systems simulated to results by Miura et al. [5]. The experiments in ref. 5 were performed at solid fractions of $0.016-0.023\%$, while our most dilute systems had $f_s = 0.017\%$ ($N_p = 2$). In agreement with the experiments, we found that at $\mathrm{Re}_{ch} = 60$, 190 only the face equilibrium positions were stable, while at $\mathrm{Re}_{ch} = 310$, 500 particles also migrated

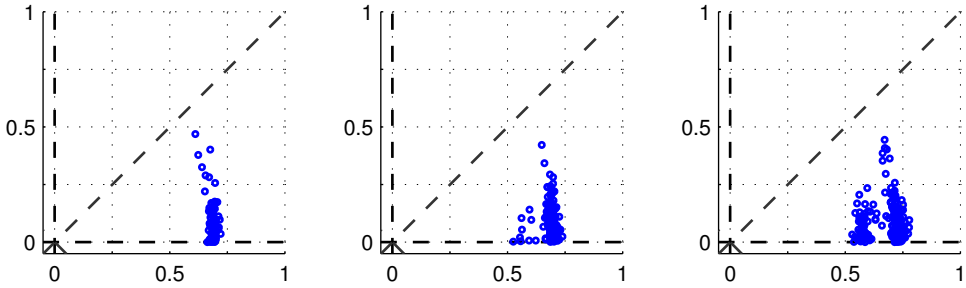

Figure 3: Equilibrium positions for $\mathrm{Re}_{\mathrm{ch}} = 60$ for $f_\mathrm{s} = 0.1\%$, 0.3%, 0.6% (left to right) folded to the grey triangle in fig. 1.

to the corner equilibrium positions. Figure 2 shows the average radial positions at the end of the simulations for the four $\mathrm{Re}_{\mathrm{ch}}$ investigated at $f_\mathrm{s} = 0.017\%$. Both corner and face positions follow the same trend as in the experiments, albeit with a slight overprediction of radial distance in our simulations. Due to the random initialization procedure, an exact determination of a focusing time was not possible. However, estimates can be made. We find focusing times of $6500 - 15000 t_\mathrm{s}$ where

$$t_\mathrm{s} = \frac{D\bar{U}}{\nu} \tag{5}$$

is the Stokes time. This is in agreement with the durations reported by Chun and Ladd [2]. Assuming that a particle travels with $\bar{U}$, the required channel lengths for full focusing range from 2.12m ($\mathrm{Re}_{\mathrm{ch}} = 500$) to 4.88m ($\mathrm{Re}_{\mathrm{ch}} = 60$), which is in good agreement with the channel length used by Miura et al. (4m).

3.2 Multi-Particle Effects

As already mentioned above, two new patterns were found in the simulations: At $\mathrm{Re}_{\mathrm{ch}} = 60$, 190, each face equilibrium position splits up in two equilibrium positions. This is shown in fig. 3. At $\mathrm{Re}_{\mathrm{ch}} = 310$, 500, a higher fraction of the particles is found at the corner equilibrium positions with increasing f_s, as illustrated in fig. 4.

3.2.1 Split equilibrium positions

At $\mathrm{Re}_{\mathrm{ch}} = 60$, 190, the equilibrium positions at the face centers split up in two equilibrium positions with increasing f_s. Figure 5 shows histograms of particles' radial distance from the channel center for these $\mathrm{Re}_{\mathrm{ch}}$. At $f_\mathrm{s} = 0.1\%$, there is only a single peak, but at $f_\mathrm{s} = 0.3\%$ a secondary peak closer to the axis appears for both

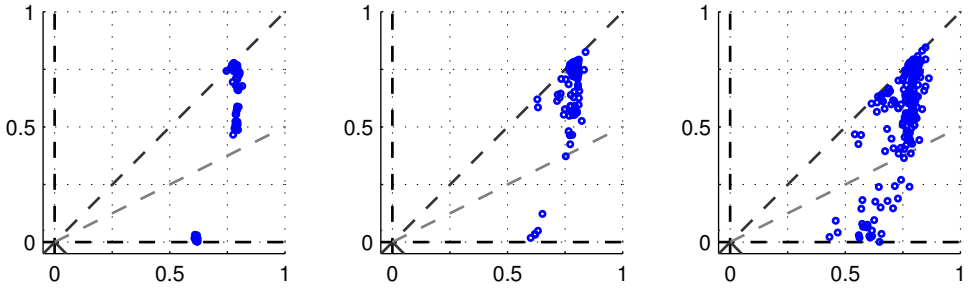

Figure 4: Equilibrium positions for $\mathrm{Re}_{\mathrm{ch}} = 310$ for $f_\mathrm{s} = 0.1\%$, 0.3%, 0.6% (left to right) folded to the grey triangle in fig. 1. Particles below the additional gray line are considered to be at the face equilibrium positions, while particles above are at the corner equilibrium positions.

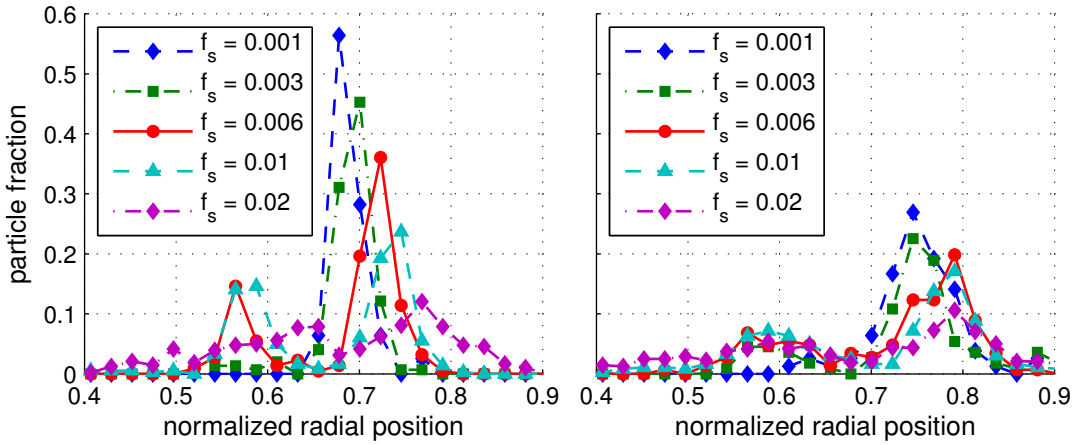

Figure 5: Normalized histograms of radial distance to the channel axis for $\mathrm{Re}_{\mathrm{ch}} = 60$ (left) and $\mathrm{Re}_{\mathrm{ch}} = 190$ (right).

$\mathrm{Re}_{\mathrm{ch}}$. The particles align in a staggered configuration as shown in fig. 6. This hints at a possible mechanism for the emergence of split equilibrium positions: Kahkeshani et al. [8] found that the preferred axial spacing between particles is smaller for staggered configurations than for particles forming a train ($2.5d_\mathrm{p}$ compared to $5d_\mathrm{p}$ in their experiments), and Humphry et al. [7] found that with increasing particle concentration, a single train in a rectangular channel will split up in two parallel trains. So, with increasing N_p, a single train becomes unstable. Due to the nature of the flow, particles are focused at the four face equilibrium positions. If now the particle density exceeds a stability limit, the average interparticle spacing goes down. To accommodate more particles in the train, a staggered configuration that allows for lower interparticle spacings is formed. We will thoroughly test this assumption

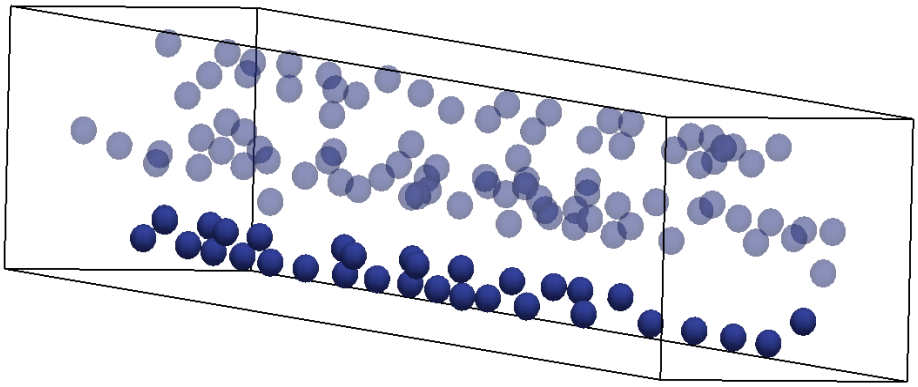

Figure 6: Illustration of the staggered configuration at $\mathrm{Re}_{\mathrm{ch}} = 60$, $f_{\mathrm{s}} = 1\%$ at the lower channel wall. Other particles have been reduced in opacity for clarity.

and publish the results in the future.

3.2.2 Instability of face equilibrium position

At $\mathrm{Re}_{\mathrm{ch}} = 310, 500$, another novel feature was found: When the number of particles in the channel was increased, a higher fraction of particles moved to the corner equilibrium position. Figure 7 (left) shows the fraction of particles at the corner equilibrium positions over f_{s}. There is a maximum at $f_{\mathrm{s}} = 0.3\%$ for $\mathrm{Re}_{\mathrm{ch}} = 310$ and at $f_{\mathrm{s}} = 0.6\%$ for $\mathrm{Re}_{\mathrm{ch}} = 500$. The minimum for $\mathrm{Re}_{\mathrm{ch}} = 500$, $f_{\mathrm{s}} = 0.03\%$ most likely comes from having not enough samples at this solid fraction. This will be investigated in the future. The patterns form in two steps: First, the particles migrate close to the equilibrium positions where they would be expected. Then, over time, particles at the face positions get pushed away and migrate to the corners, where they remain. Figure 7 (right) shows the radial positions of particles over time. Again, at the moment we can only speculate about the mechanisms leading to this effect. Nakagawa et al. [20] found that for $\mathrm{Re}_{\mathrm{ch}} > 260$ a separatrix between corner and face equilibrium positions exists, that single particles do not cross. Therefore, the initial position of a particle determines to which equilibrium position it will migrate. In the case of multiple particles, the particles travel at different velocities and constantly pass each other. When a particle passes another, there is a lateral repulsive force between the two. This lateral force could push one of the two particles over the separatrix, causing migration to another equilibrium position. It is assumed that this effect does not bring particles back to the face equilibrium positions because the corner equilibrium positions are more geometrically confined.

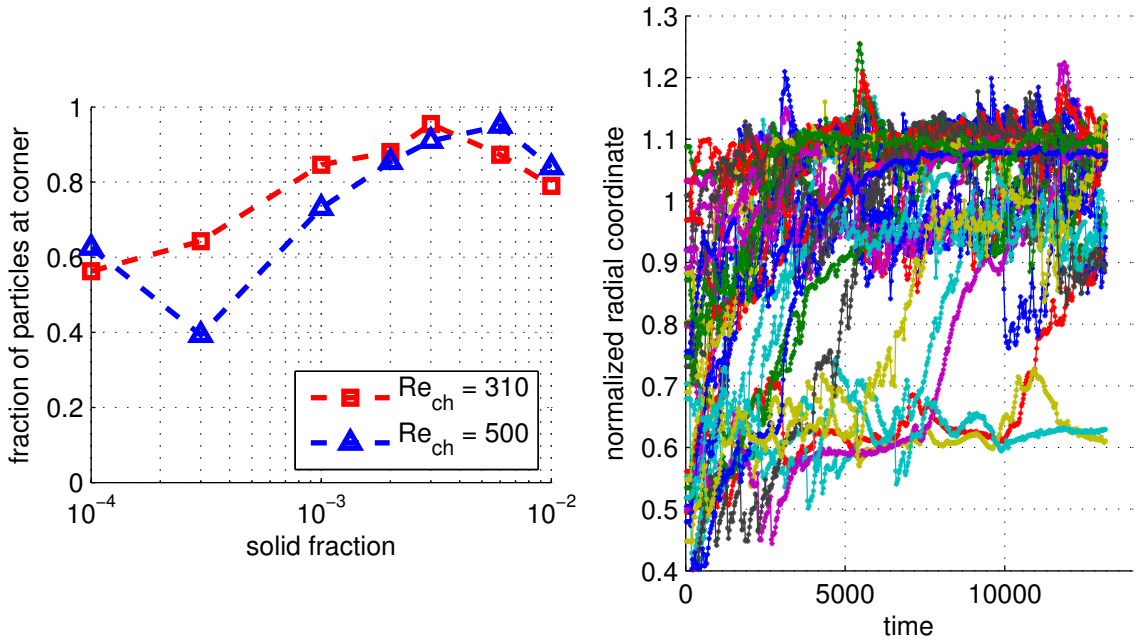

Figure 7: **Left:** Fraction of particles found at the corner equilibrium positions over $f_s$for $\mathrm{Re}_{ch} = 310, 500$. **Right:** Radial position of particles at $\mathrm{Re}_{ch} = 310$, $f_s = 0.3\%$. Time is given in multiples of Stokes time eq. (5). A radial position of ≈ 0.6 corresponds to the face equilibrium position, and a radial position of ≈ 1.1 is the corner equilibrium positions. Over time, particles migrate from the former to the latter, but not in the other direction.

4 SUMMARY AND OUTLOOK

We have looked at lateral migration phenomena in suspension flow through square channels. After making sure we match experiments for dilute cases, we increased the solid fraction. There, we found two effects: at lower Re_{ch}, a secondary equilibrium position right "on top" of the primary one appears. At $\mathrm{Re}_{ch} = 310, 500$, increasing solid fraction leads to lower occupation at the face equilibrium positions. To the best of the authors' knowledge, these effects have not been reported anywhere. A more thorough analysis of these patterns will be published soon, and we hope for independent testing of these findings, either through experiments or through numerical studies.

References

[1] G. Segré and A. Silberberg. Behaviour of macroscopic rigid spheres in poiseuille flow part 2. experimental results and interpretation. *Journal of Fluid Mechanics*, 14:136–157, 1962.

[2] B Chun and AJC Ladd. Inertial migration of neutrally buoyant particles in a square duct: An investigation of multiple equilibrium positions. *Physics of Fluids*, 18:031704, 2006.

[3] Dino Di Carlo, Daniel Irimia, Ronald G. Tompkins, and Mehmet Toner. Continuous inertial focusing, ordering, and separation of particles in microchannels. *Proceedings of the National Academy of Sciences*, 104(48):18892–18897, 2007.

[4] Dino Di Carlo, Jon F. Edd, Katherine J. Humphry, Howard A. Stone, and Mehmet Toner. Particle segregation and dynamics in confined flows. *Phys. Rev. Lett.*, 102:094503, Mar 2009.

[5] Kazuma Miura, Tomoaki Itano, and Masako Sugihara-Seki. Inertial migration of neutrally buoyant spheres in a pressure-driven flow through square channels. *Journal of Fluid Mechanics*, 749:320–330, 6 2014.

[6] Jean-Philippe Matas, Virginie Glezer, Élisabeth Guazzelli, and Jeffrey F Morris. Trains of particles in finite-reynolds-number pipe flow. *Physics of Fluids (1994-present)*, 16(11):4192–4195, 2004.

[7] Katherine J Humphry, Pandurang M Kulkarni, David A Weitz, Jeffrey F Morris, and Howard A Stone. Axial and lateral particle ordering in finite reynolds number channel flows. *Physics of Fluids*, 22(8):081703, 2010.

[8] Soroush Kahkeshani, Hamed Haddadi, and Dino Di Carlo. Preferred interparticle spacings in trains of particles in inertial microchannel flows. *Journal of Fluid Mechanics*, 786:R3, 2016.

[9] Guy R McNamara and Gianluigi Zanetti. Use of the boltzmann equation to simulate lattice-gas automata. *Physical Review Letters*, 61(20):2332–2335, 1988.

[10] Peter A Cundall and Otto DL Strack. A discrete numerical model for granular assemblies. *Geotechnique*, 29(1):47–65, 1979.

[11] D. R. Noble and J. R. Torczynski. A lattice-Boltzmann method for partially saturated computational cells. *International Journal of Modern Physics C*, 09(08):1189–1201, 1998.

[12] P. Seil and S. Pirker. LBDEMcoupling: Open-source power for fluid-particle systems. *Proceedings of the DEM7*, 2016.

[13] Philippe Seil, Stefan Pirker, and Thomas Lichtenegger. Onset of sediment transport in mono- and bidisperse beds under turbulent shear flow. *Computational Particle Mechanics*, May 2017.

[14] Timm Krüger, Halim Kusumaatmaja, Alexandr Kuzmin, Orest Shardt, Goncalo Silva, and Erlend Magnus Viggen. *The Lattice Boltzmann Method: Principles and Practice*. Springer, 2016.

[15] Thorsten Pöschel and Thomas Schwager. *Computational granular dynamics: models and algorithms*. Springer Science & Business Media, 2005.

[16] Yutaka Tsuji, Toshitsugu Tanaka, and T Ishida. Lagrangian numerical simulation of plug flow of cohesionless particles in a horizontal pipe. *Powder technology*, 71(3):239–250, 1992.

[17] D Antypov and JA Elliott. On an analytical solution for the damped hertzian spring. *EPL (Europhysics Letters)*, 94(5):50004, 2011.

[18] YC Zhou, BH Xu, AB Yu, and P Zulli. An experimental and numerical study of the angle of repose of coarse spheres. *Powder technology*, 125(1):45–54, 2002.

[19] Yunfeng Zhang and Daniel Y. Kwok. Pressure boundary conditions of the lattice boltzmann method for fully developed periodic flows. *Phys. Rev. E*, 73:047702, 2006.

[20] Naoto Nakagawa, Takuya Yabu, Ryoko Otomo, Atsushi Kase, Masato Makino, Tomoaki Itano, and Masako Sugihara-Seki. Inertial migration of a spherical particle in laminar square channel flows from low to high reynolds numbers. *Journal of Fluid Mechanics*, 779:776–793, 9 2015.